# Journal of Materials Chemistry A

Accepted Manuscript


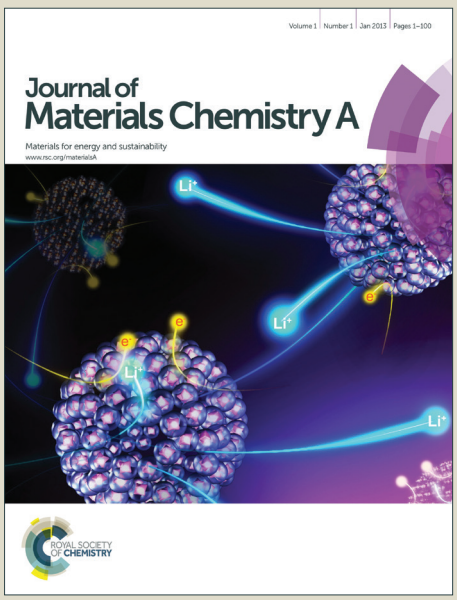





ROYAL SOCIETY OF CHEMISTRY

www.rsc.org/materialsA

Cite this: DOI: 10.1039/c0xx00000x

www.rsc.org/xxxxxx

ARTICLE TYPE

# Preparation of Multifunctional Microchannel-Network Graphene Foams

**Jun Yan,[a] Yi Ding,[a] Chuangang Hu,[a] Huhu Cheng,[a] Nan Chen,[*,a] Zhihai Feng,[b] Zhipan Zhang,[a] and Liangti Qu[*,a]**

***Received (in XXX, XXX) Xth XXXXXXXXX 20XX, Accepted Xth XXXXXXXXX 20XX***
**DOI: 10.1039/b000000x**

The new-type of multifunctional three-dimensional (3D) microchannel-network graphene foams (μCNGFs) has been facilely fabricated by using an alumina fiber blanket (AFB) template. The μCNGF with reticular space structures showed an excellent electrochemical property for electrochemical double-layer capacitors with a specific capacitance of as high as 216 $F•g^{-1}$ at a current density of 0.5 $A•g^{-1}$ in the two-electrode system. The liquid adsorption tests of various liquids further proved the outstanding adsorbing features of the μCNGF such as the fast and efficient adsorption of liquids and repeatable recyclability for petrol. The current results indicate that the μCNGF has unique advantages as a novel type of electrode material for high performance supercapacitors and is well qualified as an efficient and versatile absorber for hazardous organic liquids with potential applications in different industrial and environmental areas.

## Introduciton

Due to its unique properties such as chemical stability, catalytic activity, and excellent mechanical strength, graphene sparked such interest among the scientific and technological communities. As a result, it is known as a "wonder material". Recently, great attention [1–4] has been devoted to directly assembling low-dimensional nanocomponents, [5] e.g. the graphene sheets, into three-dimensional (3D) macroscopic porous frameworks with reticular space structures to achieve their practical applications in the fields of chemical filtering, energy storage and so on. [6–10] However, driven by the strong π-π interaction between individual graphene sheets, uncontrolled assembly of 2D graphene sheets should be avoided since the irreversible formation of graphene aggregates with small surface areas is not suitable for practical device applications where a large interface is needed. [11]

Therefore, it is of great theoretical and practical importance to develop a method to effectively interrupt the excessive aggregation of the 2D graphene sheets and thus form a reticular 3D graphene structure with desired porosity and surface area. Up to now, a number of complex methods have been developed to mitigate the aggregation of graphene sheets, including the addition of co-assembling agents to increase the interlayer distance, [12, 13] twisting the conjugated plane of graphene sheet to reduce π-π stacking, [14] and other methodologies involving template-assisted growth of 3D graphene structures. Meanwhile, the formation of 3D graphene-based macrostructures without employing interspacing agents or templates has also been reported. Li [10] and coworkers presented a bio-inspired approach to effectively prevent the restacking of chemically converted graphene sheets in multilayered films and obtained a highly porous structure with open pores generated between the sheets by colloidal interaction in the presence of water, providing the electrolyte solution with an easy access to the surface of individual sheets. As a result, this structure has made it possible to combine ultrahigh power density and high energy density in graphene-based supercapacitors and allow the device to operate at high rates. Differently, Shi [15] group prepared a self-assembled graphene hydrogel (SGH) via a one-step hydrothermal process by heating homogeneous graphene oxide aqueous dispersion in an autoclave. Nonetheless, it is still of a great challenge to find a simple strategy to mass-produce graphene macrostructures with a satisfactory porosity and desirable flexibility.

Electrochemical supercapacitors have been widely studied in recent years, owing to their relatively high power density and long cycle life. Carbonaceous materials such as carbon nanotubes (CNTs) and graphenes are among the most frequently used types of electrode materials for supercapacitors [10, 16, 17] In particular, reduced graphene oxides (rGOs) [18, 19] have received increasing attentions due to its inexpensive preparation from graphene oxides (GOs) and facile modifications through chemical functionalizations [20, 21] Consequently, 3D graphene macroscopic frameworks have been considered as ideal candidates for electrode materials in electrochemical supercapacitors, because they enable the integration of nanoscale features into 3D macroscopic architecture [10, 22–24] and render electrodes with fast electron/ionic transfer properties for high energy storage capacities.

In the current work, we have developed a simple method for large-scale preparation of the new-type of microchannel-network graphene foams (μCNGFs). GO was first adsorbed onto the AFB that served as a template, which was then annealed to reduce GO

to rGO. μCNGF was finally obtained after removing the AFB template. Results have shown that the method established hereby is an attractive tool to fabricate 3D reticular microchannels graphenes with a high electrochemical/ thermal stability and an excellent adsorption performance for organic solvents.

## Experimental Section

### Characterization of μCNGF

The as-prepared 3D μCNGF foams were characterized by the Scanning Electron Microscope (SEM, JSM-7500F) and the Transmission Electron Microscopy (TEM, JEM-2010). Raman spectra were measured by using a RM 2000 microscopic confocal Raman spectrometer (Renishaw PLC, England) with a 514 nm laser as the excitation source and the Philips PW-1710 Diffractometer were also used. The specific surface area of all the samples were analyzed by BET surface area analyzer (3H-2000PS1, Beishide Instrument-S&T. Co., Ltd. Beijing).

### Electrochemical experiments

Electrochemical properties of the electrodes were measured by CHI 660D electrochemical workstation under ambient conditions. In this study, the typical three electrode system in a three-electrode cell with 1 M $LiClO_4$ electrolyte was used, in which Pt foil was used as the counter electrode, the μCNGF electrode as the working electrode and an Ag/AgCl electrode as the reference electrode. To build a two-electrode testing system, two identical μCNGF electrodes were separated by a porous membrane (pore sizes of 8 μm with a thickness of 40 μm) soaked with 1 mol/L $LiClO_4$. Cyclic voltammetry (CV) and charge/discharge curves at different current density were all measured with a potential range of 0–0.8 V.

### Solvent adsorption experiments

We selected some common organic liquids to test the adsorption capacity of the μCNGF. With their densities listed in the bracket, these liquids are methanol (0.792 g $cm^{-3}$), ethanol (0.789 g $cm^{-3}$), acetone (0.786 g $cm^{-3}$), tetrahydrofuran (0.883 g $cm^{-3}$), toluene (0.867 g $cm^{-3}$), chloroform (1.476 g $cm^{-3}$), dichloromethane (1.326 g $cm^{-3}$), tetrachloromethane (1.5867 g $cm^{-3}$), cyclohexane (0.778 g $cm^{-3}$), *n*-propanol (0.805 g $cm^{-3}$), isopropyl alcohol (0.786 g $cm^{-3}$), petroleum ether (0.640 g $cm^{-3}$), olive oil (0.918 g $cm^{-3}$), gasoline (0.825 g $cm^{-3}$) and pump oil (0.879 g $cm^{-3}$). The recycling of the μCNGF was carried out by burning the μCNGF in flames to remove the organic liquid and restore its original adsorption capacity. Typically for each organic liquid, the μCNGF was recycled for more than 65 times to evaluate its recyclability.

## Result and Discussion

### Compositional and structural analyses

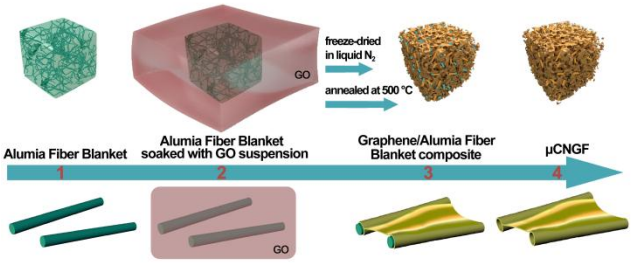


**Scheme 1.** Cartoonic presentation of μCNGF preparation. (1) AFB; (2) AFB soaked with GO suspension; (3) the graphene/AFB composite; (4) The as-prepared μCNGF after the removal AFB. The upper and the lower part depict the process from the view of whole AFB and individual alumina fibers, respectively.

Scheme 1 depicts different stages during the preparation process of the μCNGF, while the detailed fabrication of GO are shown in the Supporting Information. The AFB was initially put in a homogeneous GO aqueous solution (6 mg•$mL^{-1}$) for 0.5 h to sufficiently absorb the GO suspension (Stage 1 and 2). The GO/AFB composite was then annealed in the nitrogen atmosphere at 500 ℃ for 2 h to reduce the GO into rGO attached to the AFB (Stage 3). The AFB was finally removed with 10 % hydrofluoric acid (weight percentage, bought from Beijing chemical reagent company), then repeated washing with deionized water to remove all the acid followed by lyophilization for the pure μCNGF.

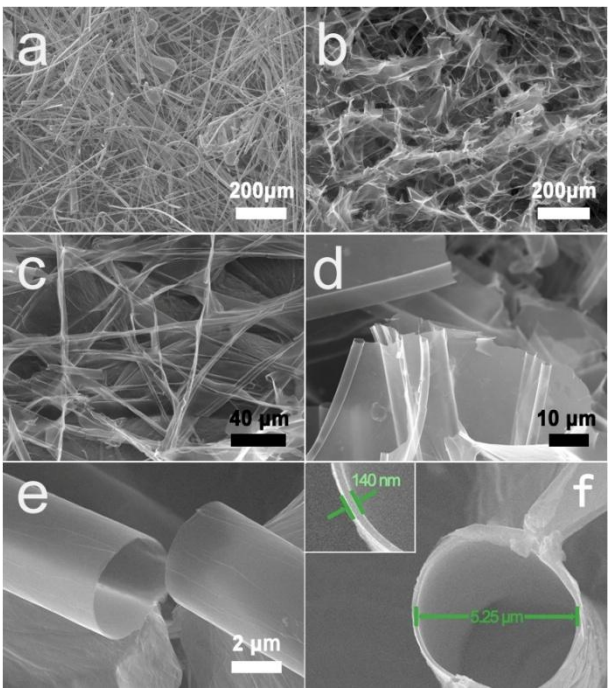


**Figure 1.** (a) SEM image of AFB; (b)-(f) SEM images of the μCNGF under different magnifications, where (b), (c), and (d) are cross-section images of the μCNGF.

The morphologies of the AFB and the as-formed μCNGF are shown in Figure 1 at different magnifications. Figure 1a is a typical SEM image of the AFB and it can be seen that the

alumina fiber featured a very smooth surface and a high length-to-width ratio with a diameter approximately ranging from 4 to 10 μm, ideally serving as a template for preparing interconnected reticular structures. Due to the presence of hydroxyl groups on their surfaces, the alumina fibers are known to be hydrophilic, therefore GO can be conveniently adsorbed onto the AFB template through its hydroxyl, carboxyl, and/or epoxy groups during soaking the AFB in the GO solution (Stage 2, Scheme 1). In addition, driven by the capillary force, the GO solution could also penetrate the AFB template and fill in the voids between the alumina fibers. The water evaporation in the subsequent thermal reduction process (Stage 3, Scheme 1) would consequently leave a lateral graphene connection between the graphene-coated alumina fibers, resulting in the formation of an interconnected 3D continuous microchannel graphene structure, μCNGF, after the removal of the AFB template (Figure 1b). For practical purposes we have calculated the surface area per unit volume of μCNGF, shown in the Supporting Information of section S4. Meanwhile, the porosity values are also calculated.

The porous microchannels of the μCNGF are more clearly seen in Figure 1d, which is an enlarged image of the same region of the μCNGF in Figure 1c. With the aid of the AFB as the sacrificial template, graphene sheets mostly conform to the shape of original alumina fibers, thus overcoming the restacking of graphene sheets and forming continuously cross-linked microchannels. Such a structure would provide better conductive contacts between the graphene sheets and lower the series resistance of the μCNGF. Figure 1e is an image of a broken microchannel in the μCNGF, showing its smooth inner and outer walls of the tubular structure. The wall thickness of the microchannel was determined to be 140 nm (Figure 1f), suggesting its controlled formation from multilayer aggregation of GO sheets. The diameter of the tube was measured to be around 5 μm, well corresponding to the diameter range of alumina fibers displayed in Figure 1a.

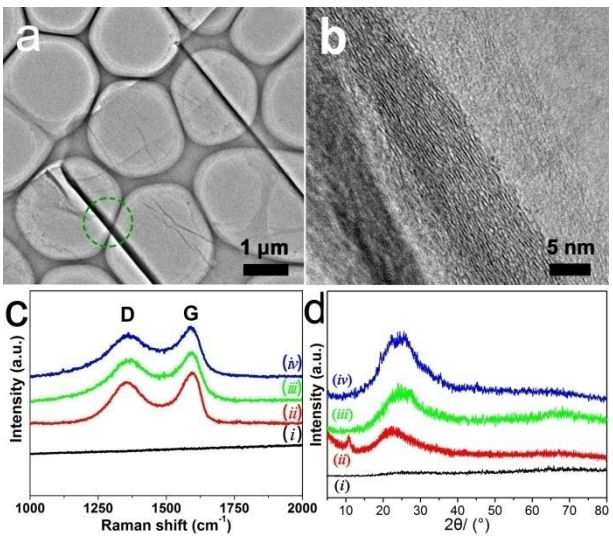


**Figure 2.** (a) The TEM image of μCNGF and (b) magnification of the dotted circle area in (a). (c) and (d) are the Raman spectra and XRD curves of (*i*) AFB, (*ii*) GO/AFB, (*iii*) rGO/AFB, and (*iv*) μCNGF, respectively.

The TEM images of μCNGF are shown in Figure 2 to further prove its hollow nature. As demonstrated in Figure 2a, graphene sheets formed microchannels with the diameter of about 5 μm, in consistence with the SEM observation in Figure 1f. Under a larger magnification (Figure 2b), it is apparent that the walls of the microchannel had a distinct layered structure, confirming the μCNGF was assembled from graphene sheets through the interlayer stacking process. The presence of the AFB template confined the assembling of individual graphene sheets specifically on or within the vicinity of the alumina fibers and thus effectively prevented further aggregation of graphene sheets to chunky materials.

Raman spectroscopy has historically played an important role in the structural characterization of graphitic materials. Graphene materials are known to have characteristic Raman features of D band (1356 $cm^{-1}$) and G band (1595 $cm^{-1}$). The D and G bands originate from the disorder band caused by the graphite edges and the in-phase vibration of the graphite lattice, respectively, and the relative intensity ratio of D-band and the G-band ($I_D/I_G$) is an indicator of GQD edge-quality. As can be seen from trace (*i*) in Figure 2c, the AFB sample literally had no discernible Raman peaks. With the adsorption of GO, samples (*ii*) clearly showed G and D Raman peaks in the Raman spectrum and proved the adhesion of GO on the AFB. The decrease in the intensity ratio, $I_D/I_G$, of sample (*iii*) and (*iv*) (0.89) compared with sample (*ii*) (0.98) was probably caused by the thermal reduction reaction as has been reported by other researchers [25, 26].

The XRD analysis further shows the formation of microchannels by the graphene sheets. Samples (*ii*), (*iii*) and (*iv*) all showed the XRD diffraction peak at 2θ of 25.4°, corresponding to an interlayer spacing of 0.35 nm between graphite layers, while sample (*ii*) have a clear diffraction peak of graphene oxide at around 11 °. After the thermal annealing, the enhanced XRD peak intensities at 2θ of 25.4° in samples (*iv*) compared with sample (*ii*) suggest the successful reduction of GO to rGO and thus the improvement in the crystallinity of the graphene material, verifying that the μCNGF was formed by crystalline graphene sheets.

The establishment of such an interconnected porous 3D structure like μCNGF has great potentials in flexible energy-storage devices such as electrochemical supercapacitors (the μCNGF cyclic voltammetry of before and after bending are shown in Supporting Information, section S3). In principle, the obtained interconnected micron-sized channels in the μCNGF can simultaneously provide sufficient pathways for the ion diffusions and facilitate the charge transportation in the electrochemical supercapacitors.[27, 28] Additionally, the excellent mechanical properties of the μCNGF, as shown in Figure 3c, can realize the fabrication of flexible supercapacitors. In addition, the electrical test showed the pure μCNGF a good conductivity of 13.6 S•$cm^{-1}$.

**Electrochemical Properties**

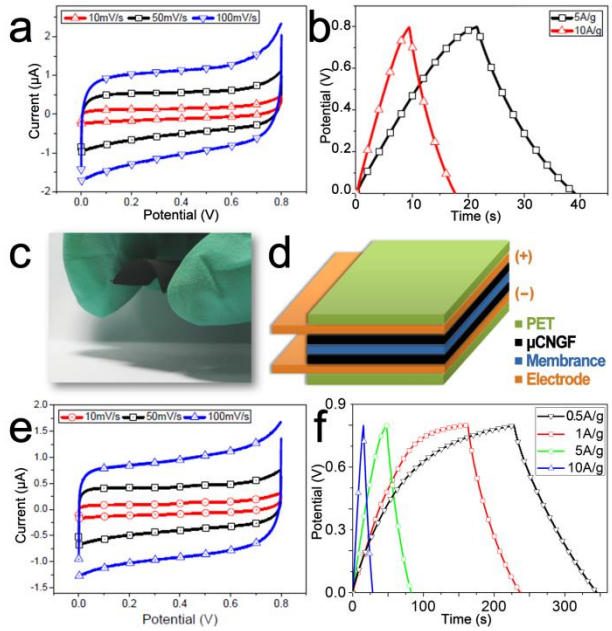


**Figure 3.** (a) CV curves of a μCNGF electrode in 1M $LiClO_4$ aqueous solution in a three-electrode system at different scan rates of 10 mV•s$^{-1}$, 50 mV•s$^{-1}$, and 100 mV•s$^{-1}$, respectively; (b) The galvanostatic charge-discharge curves at a current density of 5 and 10 A•g$^{-1}$, respectively. (c) The μCNGF under the bent state. (d) Schematic illustration of the μCNGF supercapacitor. (e) CV curves of a μCNGF electrode in 1M $LiClO_4$ aqueous solution in a two-electrode system at different scan rates of 10 mV•s$^{-1}$, 50 mV•s$^{-1}$, and 100 mV•s$^{-1}$, respectively. (f) The galvanostatic charge-discharge curves at a current density of 0.5 A•g$^{-1}$, 1 A•g$^{-1}$, 5 A•g$^{-1}$, and 10 A•g$^{-1}$, respectively.

Figure 3a shows the cyclic voltammogram (CV) curves of the μCNGF electrode in a three-electrode system under different scan rates. The shape of the CV curves does not change notably with the increasing scan rate from 10 to 100 mV•s$^{-1}$ and the rectangular-like shape indicates the excellent capacitive behaviors of the assembled supercapacitor. Accordingly, the galvanostatic charge-discharge curves at different current densities in Figure 3b exhibit a symmetric triangle feature without an obvious potential drop (IR drop) [29] and the capacitance could reach 125 F•g$^{-1}$ at a high current density of 5 A•g$^{-1}$. Specific capacitance at different areal densities are also discussed. The areal densities had little effect on the specific capacitance (as shown in the supporting information, section S9).

We also tested the electrochemical performance of the μCNGF in a two-electrode configuration. A symmetric supercapacitor was thus constructed by first sandwiching a membrane soaked with 1 mol•L$^{-1}$ of $LiClO_4$ between two identical pieces of μCNGFs and then encapsulating the device by polyethylene terephthalate (PET) membranes (Figure 3d). As shown in Figure 3e, the CV curves of the μCNGF electrode under different scan rates again remain in an approximately rectangular shape, characteristic of the ideal double-layer capacitor. Based on the charge-discharge curves, as shown in Figure 3f, the specific capacitances of the μCNGF was calculated to be about 216 F•g$^{-1}$ at a current density of 0.5 A•g$^{-1}$, which was higher than those of the 3D pure graphene foam (*ca.* 110 F•g$^{-1}$) [30] and the graphene paper (*ca.* 122 F•g$^{-1}$) [31] based electrodes. Besides, Nyquist plot for μCNGF supercapacitor carried out in electrochemical impedance spectroscopy (EIS) test was in agreement with the above observation as shown in the supporting information. The equivalent series resistance obtained from the x-intercept of the Nyquist plot (Figure S7 inset, supporting information) was low at ~3.5 Ω, suggesting that the μCNGF electrodes have small resistance with good ion response. This improvement in specific capacitance could be ascribed to the construction of an ideal interface for supercapacitors where the graphene sheets were highly exposed to the electrolyte in the interconnected microchannel structure of μCNGF [32, 33] and the additional electrolytic pathways which were provided by microchannel, indicating that the μCNGF has unique advantages as a novel type of electrode material or supporting material for high performance supercapacitors. Specifically, the microchannel increased the electrode-to-electrolyte contact area and enable ions to intercalate with the graphene sheets.

### Adsorption of Organic Solvents

Meanwhile, the unique porous structure of the μCNGF endows it with a low density. As listed in Table 1, the μCNGF features a density of 6.2 mg cm$^{-3}$, a value among one of the lowest for 3D graphene foams and aerogels reported so far, qualifying it as a competitive candidate with a high specific capacity in the ultra-selective adsorption of organic solvents.

**Table 1.** The density of typical 3D graphene materials

| Sample | Method | Density (mg cm$^{-3}$) | Ref. |
|---|---|---|---|
| this work | Template | 6.2 | |
| graphite foam | template, CVD | 9.6-20 | [34-36] |
| graphene oxide foam | hydrothermal | 8-30 | [30, 38, 39] |
| graphene foam | hydrothermal, CVD | 5-12 | [40, 41] |
| graphene aerogel | sol-gel | 8.3-96 | [42-46] |
| 3D graphene | CVD | 5.15-22 | [47, 48] |
| 3D graphene | hydrothermal | 15-30 | [49, 50] |
| 3D graphene | chemical reduction | 18 | [51] |
| 3D graphene | sol-gel | 16-25 | [52] |
| 3D graphene | self-assembly | 80-100 | [53] |

**Table 2.** Adsorption capacities of some graphene and other carbon-base materials

| Sample | Adsorbent | Adsorption capacity(g/g) | Ref. |
|---|---|---|---|
| this work | various organic solvents and oils | 137-760 | |
| graphene oxide foam | motor oils, cyclohexane, etc | 10-370 | [30, 54, 55] |
| graphene aerogel | cyclohexane, toluene, gasoline, etc | 13-27 | [56] |
| graphene foam | cyclohexane, etc | 20-86 | [41] |
| CNF hydrogel | toluene, petrol, etc | 40-115 | [57] |
| CNTs Sponge/Aerogels | petrol, ethanol, etc | 80-320 | [58-60] |
| exfoliated graphite | heavy oil | 80-90 | [61] |
| activated carbons | benzene, toluene | <1 | [62] |
| graphene-based composite | motor oils, ethanol, etc | 80-600 | [63-66] |

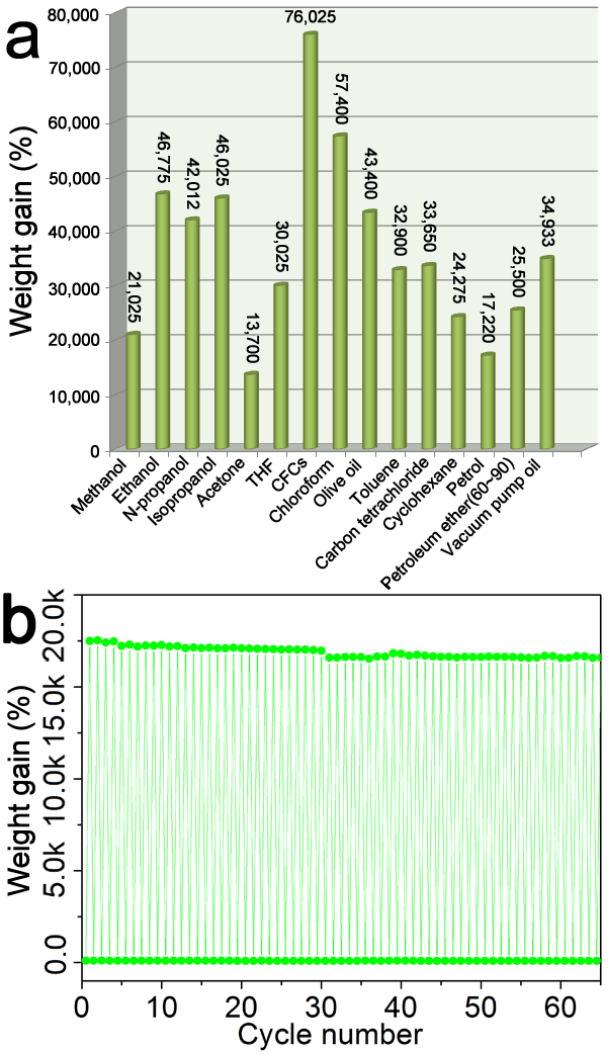


**Figure 4**. (a) The weight gain percentage of the μCNGF in different organic solvents; (b) Weight gain of the μCNGF in the recyclability test. The μCNGF repetitively adsorbed and released petrol for more than 65 cycles, where the petrol was directly burned from the μCNGF during each recycling.

As shown in Figure 4a, the μCNGF demonstrated high specific adsorption capacities (defined by weight gain percentage, which is the ratio between the mass of the adsorbent and the weight of the dry μCNGF) for a wide range of organic solvents. Impressively, the μCNGF could adsorb dichloromethane up to 760 times of its own weight and the weight gain ratio was from 137 to 534 for a series of other common organic solvents ranging from acetone to chloroform. Compared to other carbon-based materials listed in Table 2, the adsorption performance of the μCNGF is superior in the uptake of different solvents, presumably due to the highly porous and interconnecting nature of the μCNGF. The recyclability test of the μCNGF was performed with petrol as the adsorbent and the weight of the original μCNGF was closely monitored. The adsorption ability of the μCNGF remained essentially unchanged after more than 65 cycles basically. As demonstrated in Figure 4b, the μCNGF showed less than 5 % change in its adsorption capacity of petrol in 65 cycles, suggesting the robustness and outstanding recyclability of the μCNGF. No visual damage to the μCNGF could be observed after the long time cycling test, validating the μCNGF as an excellent material to adsorb organic solvents in the fields of waste disposal and sewage separation.

## Conclusion

In summary, we have successfully prepared multifunctional μCNGFs from GO suspensions using the alumina fiber blanket as the template. The μCNGF with interconnected reticular structures showed an excellent electrochemical capacitance of 216 $F \bullet g^{-1}$ at a current density of 0.5 $A \bullet g^{-1}$ in the two-electrode system. In addition, the μCNGF could efficiently adsorb a range of common organic solvents with an excellent recyclability. Probably, the facile preparation of the μCNGF can be scalable to industrial levels, therefore the multifunctional μCNGF has a strong potential to become a versatile and efficient material for electrochemical supercapacitors and organic waste adsorption.

## Acknowledgment

This project is sponsored by NSFC (No. 21325415, 21174019, 21301018, 51161120361), National Basic Research Program of China (2011CB013000, 2011CB605802), Basic Research Foundation of Beijing Institute of Technology (20121942008), Fok Ying Tong Education Foundation (No. 131043), the 111 Project B07012, and the Beijing Key Laboratory for Chemical Power Source and Green Catalysis under the contract no. 2013CX02031.

## Notes and references

[a] *Key Laboratory of Cluster Science, Ministry of Education of China; Beijing Key Laboratory of Photoelectronic/Electrophotonic Conversion Materials, School of Chemistry, Beijing Institute of Technology, Beijing 100081, P. R. China.*

[b] *State Key Laboratory of Advanced Functional Composite Materials, Aerospace Research Institute of Materials and Processing Technology, Beijing 100076, P. R. China*

† Electronic Supplementary Information (ESI) available: detailed fabrication, electrical property of pure μCNGF, cyclic voltammetry of the flexible supercapacitors, specific surface area, porosity analysis, nitrogen adsorption-desorption isotherm, pore size distribution curve, cyclic stability, specific capacitance at different areal densities and different scan rates, Nyquist plots, and XPS analysis of μCNGFs. See DOI: 10.1039/b000000x/

‡ Footnotes should appear here. These might include comments relevant to but not central to the matter under discussion, limited experimental and spectral data, and crystallographic data.

1 K. Ariga, T. Mori and J. Hill, *Adv. Mater.* 2012, **24**, 158.
2 K. Sakakibara, J. Hill and K. Ariga, *Small* 2011, **7**, 1288.
3 K. Ariga, A. Vinu, Y. Yamauchi and Q. Ji Hill, J. *Bull. Chem. Soc. Jpn.* 2012, **85**, 1.
4 M. Osada and T. Sasaki, *Adv. Mater.* 2012, **24**, 210.
5 N. Chen, S. Chen, C. Ouyang, Y. Yu, T. Liu and Y. Li, *NPG Asia Mater.* 2013, 5, e59. doi:10.1038/am.2013.36.
6 U. Maiti, J. Lim, K. Lee, W. Lee and Sang Ouk Kim, *Adv. Mater.* 2014, **26**, 615.
7 U. Maiti, W. Lee, J. Lee, Y. Oh, J. Kim, J. Kim, J. Shim, T. Han and S. Kim, *Adv. Mater.* 2014, **26**, 40.
8 W. Lee, T. Hwang, J. Hwang, H. Kim, J. Lim, H. Jeong, J. Shim, T. Han, J. Kim, J. Choi and S. Kim, *Energy Environ. Sci.* 2014, **7**, 621.
9 S. Yin, Y. Zhang, J. Kong, C. Zou, C. Li, X. Lu, J. Ma, F. Boey and X. Chen, *ACS Nano* 2011, **5**, 3831.
10 X. Yang, J. Zhu, L. Qiu and D. Li, *Adv. Mater.* 2011, **23**, 2833–2838.
11 Z. Fan, J. Yan, L. Zhi, Q. Zhang, T. Wei, J. Feng, M. Zhang, W. Qian and F. Wei, *Adv. Mater.* 2010, **22**, 3723.
12 C. Liu, K. Wang, S. Luo, Y. Tang and L. Chen, *Small* 2011, **7**, 1203.
13 V. Tung, J. Huang, I. Tevis, F. Kim, J. Kim, C. Chu, S. Stupp and J. Huang, *J. Am. Chem. Soc.* 2011, **133**, 4940.
14 X. Cao, Y. Shi, W. Shi, G. Lu, X. Huang, Q. Yan, Q. Zhang and H. Zhang, *Small* 2011, **7**, 3163.
15 Y. Xu, K. Sheng, C. Li and G. Shi, *ACS Nano* 2010, **4**, 4324.
16 B. Luo, S. Liu, L. Zhi, *Small* 2012, **8**, 630.
17 Y. Zhu, S. Murali, M. Stoller, K. Ganesh, W. Cai, P. Ferreira, A. Pirkle, R. Wallace, K. Cychosz, M. Thommes, D. Su, E. Stach and R. Ruoff, *Science* 2011, **332**, 1537.
18 H. Bai. C. Li and G. Shi, *Adv. Mater.* 2011, **23**, 1089.
19 L. Zhang, R. Zhou and X. Zhao, *J. Mater. Chem.* 2010, **20**, 5983.
20 F. Liu, S. Song, D. Xue and H. Zhang, *Adv. Mater.* 2012, **24**, 1089.
21 M. Segal, *Nat. Nanotechnol.* 2009, **4**, 612.
22 F. Du, D. Yu, L. Dai, S. Ganguli, V. Varshney and A. Roy, *Chem. Mater.* 2011, **23**, 4810.
23 B. Choi, M. Yang, W. Hong, J. Choi and Y Huh,. *ACS Nano* 2012, **6**, 4020.
24 D. Marcano, D. Kosynkin, J. Berlin, A. Sinitskii, Z. Sun, A. Slesarev, L. Alemany, W. Lu and J. Tour, *ACS Nano* 2010, **4**, 4806.
25 A. Eng, H. Poh, F. Šaněk, M. Maryško, S. Matějková, Z. Sofer and P. Martin, *ACS Nano* 2013, **7**, 5930.
26 T. Zhang, X. Li, S. Kang, L. Qin, G. Li and J. Mu, *J. Mater. Chem.* A 2014, **2**, 2952.
27 T. Kim, G. Jung, S. Yoo, K. Suh and R. Ruoff, *ACS Nano* 2013, **7**, 6899.
28 L. Yang, S. Cheng, Y. Ding, X. Zhu, Z. Wang and M. Liu, *Nano Lett.* 2012, **12**, 321.
29 Y. Sun, Q. Wu and G. Shi, *Energy Environ. Sci.* 2011, **4**, 1113.
30 Z. Niu, J. Chen, H. Hng, J. Ma and X. Chen, *Adv. Mater.* 2012, **24**, 4144.
31 Y. Zhu, M. Stoller, W. Cai, A. Velamakanni, R. Piner, D. Chen and R. Ruoff, *ACS Nano* 2010, **4**, 1227.
32 Z. Wu, A. Winter, L. Chen, Y. Sun, A. Turchanin, X. Feng and K. Müllen, *Adv. Mater.* 2012, **24**, 5130.
33 L. Sun, L. Wang, C. Tian, T. Tan, Y. Xie, K. Shi, M. Li and H. Fu, *RSC Adv.* 2012, **2**, 4498.
34 H. Ji, L. Zhang, M. Pettes, H. Li, S. Chen, L. Shi, R. Piner and R. Ruoff, *Nano Lett.* 2012, **12**, 2446.
35 J. Ji, L. Zhang, H. Ji, Y. Li, X. Zhao, X. Bai, X. Fan, F. Zhang and R. Ruoff, *ACS Nano* 2013, **7**, 6237.
36 M. Pettes, H. Ji, R. Ruoff and L. Shi, *Nano Lett.* 2012, **12**, 2959.
37 L. Imperiali, C. Clasen, J. Fransaer, C. Macosko and J. Vermant, *Mater. Horiz.* 2014, **1**, 139.
38 J. Kuang, L. Liu, Y. Gao, D. Zhou, Z. Chen, B. Han and Z. Zhang, *Nanoscale* 2013, **5**, 12171.
39 T. Wu, M. Chen, L. Zhang, Y. Liu, J. Yan, W. Wang and J. Gao, *J. Mater. Chem. A* 2013, **1**, 7612.
40 H. Bi, X. Xie, K. Yin, Y. Zhou, S. Wan, L. He, F. Xu, F. Banhart and L. Sun, Ruoff, R. *Adv. Funct. Mater.* 2012, **22**, 4421.
41 Z. Chen, W. Ren, L. Gao, B. Liu, S. Pei and H. Cheng, *Nature Mater.* 2011, **10**, 424.
42 Z. Xu, Y. Zhang, P. Li and C. Gao, *ACS Nano* 2012, **6**, 7103.
43 S. Nguyen, H. Nguyen, A. Rinaldi, N. Nguyen and Z. Duong, *Colloids and Surfaces A: Physicochem. Eng. Aspects* 2012, **414**, 352.
44 H. Hu, Z. Zhao, W. Wan, Y. Gogotsi and J. Qiu, *Adv. Mater.* 2013, **25**, 2219.
45 J. Wang, Z. Shi, J. Fan, Y. Ge, J. Yin and G Hu,. *J. Mater. Chem.* 2012, **22**, 22459.
46 S. Jung, H. Jung, M. Dresselhaus, Y. Jung and J. Kong, *Sci. Rep.* 2012, **2**, 849.
47 H. Bi, F. Huang, J. Liang, Y. Tang, X. Lu, X. Xie and M. Jiang, *J. Mater. Chem.* 2011, 21, 17366.
48 W. Li, S. Gao, L. Wu, S. Qiu, Guo. Y, X. Geng, M. Chen, S. Liao, C. Zhu, Y. Gong, M. Long, J. Xu, X. Wei, M. Sun and L. Liu, *Sci. Rep.* 2013, **3**, 2125.
49 Z. Tang, S. Shen, J. Zhuang and X. Wang, *Angew. Chem. Int. Ed.* 2010, **49**, 4603.
50 Y. Zhao, J. Liu, Y. Hu, H. Cheng, C. Hu, C. Jiang, L. Jiang, A. Cao and L. Qu, *Adv. Mater.* 2013, **25**, 591.
51 W. Chen and L. Yan, *Nanoscale* 2011, **3**, 3132.
52 M. Worsley, T. Olson, J. Lee, T. Willey, M. Nielsen, S. Roberts, P. Pauzauskie, J. Biener, J. Satcher and T. Baumann, *J. Phys. Chem. Lett.* 2011, **2**, 921.
53 M. Worsley, S. Kucheyev, H. Mason, M. Merrill, B. Mayer, J. Lewicki, C. Valdez, M. Suss, M. Stadermann, P. Pauzauskie, J. Satcher, J. Biener and T. Baumann, *Chem. Commun.* 2012, **48**, 8428.
54 S. Park, S. Kang, E. Jung, S. Park and H. Park, *RSC Adv.* 2014, **4**, 899.
55 Y. He, Y. Liu, T. Wu, J. Ma, X. Wang, Q. Gong, W. Kong, F. Xing, Y. Liu and J. Gao, *J. Hazard Mater.* 2013, **260**, 796.
56 H. Cong, X. Ren, P. Wang, S. Yu, *ACS Nano* 2012, **6**, 2693.
57 H. Liang, Q. Guan, L. Chen, Z. Zhu, W. Zhang, S. Yu, *Angew. Chem. Int. Ed.* 2012, **51**, 5101.
58 X. Gui, J. Wei, K. Wang, A. Cao, H. Zhu, Y. Jia, Q. Shu and D. Wu, *Adv. Mater.* 2010, **22**, 617.
59 H. Sun, Z. Xu and C. Gao, *Adv. Mater.* 2013, **25**, 2554.
60 X. Gui, Z. Zeng, Z. Lin, Q. Gan, R. Xiang, Y. Zhu, A. Cao and Z. Tang, *ACS Appl. Mater. Interf.* 2013, **5**, 5845.
61 M. Toyoda and M. Inagaki, *Carbon* 2000, **38**, 199.
62 M. Lillo–Ródenas, D. Cazorla–Amorós and A. Linares–Solano, *Carbon* 2005, **43**, 1758.
63 S. Li, S. Tian, Y. Feng, J. Lei, P. Wang and Y. Xiong, *J. Hazardous Mater.* 2010, **183**, 506.
64 X. Dong, J. Chen, Y. Ma, J. Wang, M. Chan–Park, X. Liu, L. Wang, W. Huang and P. Chen, *Chem. Commun.* 2012, **48**, 10660.
65 Y. Zhao, C. Hu, Y. Hu, H. Cheng, G. Shi and L. Qu. *Angew. Chem. Int. Ed.* 2012, **124**, 11533.
66 H. Li, L. Liu and F. Yang, *J. Mater. Chem. A* 2013, **1**, 3446.

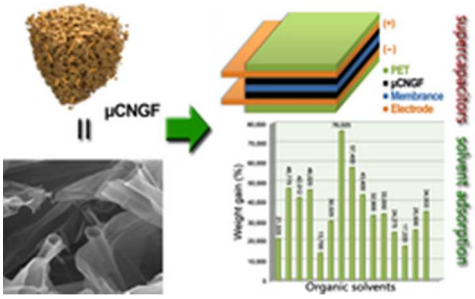


19x12mm (300 x 300 DPI)

A three-dimensional microchannel-network graphene foams with high performance supercapacitors and excellent adsorption function was fabricated.